Geometrical analysis of the electro-optical effect in nematic droplets

L. Jiménez
Instituto de Física, Universidad Nacional Autónoma de México, Apdo. Postal 20-364, 01000 México, D.F., Mexico

Carlos I. Mendoza*
Instituto de Investigaciones en Materiales, Universidad Nacional Autónoma de México, Apdo. Postal 70-360, 04510 México, D.F., Mexico

J. A. Reyes
Instituto de Física, Universidad Nacional Autónoma de México, Apdo. Postal 20-364, 01000 México, D.F., Mexico
(Received 13 May 2005; published 9 November 2005)

Using the boundary-layer approach, we study the radial-axial transition in a nematic sphere in the presence of an external field. We calculate analytically an asymptotic expression for the nematic configuration subject to an external low frequency field. Then, we consider an incident plane wave crossing a nematic droplet immersed in an isotropic matrix under the presence of a low frequency field. We calculate the ray trajectories within the optical limit for various values of the external field and find the ray deviation as a function of the incident position parametrized by the magnitude of the field.

DOI: 10.1103/PhysRevE.72.051705 PACS number(s): 61.30.Gd, 64.70.Md, 61.30.Jf

I. INTRODUCTION

The development of polymer-dispersed liquid crystals (PDLCs), which are dispersions of liquid crystal rich droplets in a polymer matrix [1], has brought a great deal of interest in the study of light propagation in spherical geometries. The size of spherical droplets in these materials is usually uniform but can vary between 0.1 and 10 μm. The nematic configuration within droplets depends on the surface anchoring and elastic constants, and is responsible for the refractive and birefringent properties of the droplets. It should be mentioned that the electro-optical effect of PDLCs is one of the reasons for their potential applicability in different devices [2,3]. This effect consists in a change of appearance of the PDLC cell from turbid to transparent, after applying a low frequency electric field to the cell plates.

There are some pioneering works [4,5] devoted to analyzing light scattering from a nematic droplet. Two complementary physical limits were considered in these works, namely, the Rayleigh-Gans approximation and the anomalous-diffraction approach which assume, respectively, a much smaller and much larger droplet radius than the wavelength of the light, and also both of them suppose a small dielectric anisotropy. For the latter work these assumptions allow the author to consider the light as a ray which does not change its direction but only suffers a change of phase, that is to say, the refractive effects which stem from the local changes of the refraction index induced by the nematic configuration are completely neglected. These refractive effects are expected to be important in birefringent and inhomogeneous media like liquid crystals even for moderate dielectric anisotropy values, and are able to curve the trajectory of light beams as well as induce local changes of phase instead of a global one, which can develop richer diffraction patterns.

The purpose of this work is to study this refractive effects by calculating the ray trajectories corresponding to the transverse electric and magnetic modes when propagating in a nematic droplet, in the limit of geometrical optics. More specifically, we shall calculate the ray trajectories of an initially plane wave when it enters and emerges from a nematic droplet with homeotropic alignment and under the action of an external uniform low frequency field.

The outline of the paper is as follows. In Sec. II we derive an analytical approximation for describing the polar dependence for the nematic droplet structure in the presence of an external field. In Sec. III we apply the boundary-layer theory to find the asymptotic radial dependence of the nematic configuration. In Sec. IV we discuss the transverse magnetic and electric eikonal equations valid in the limit of geometrical optics. In Sec. V we calculate the ray trajectories for the radial and axial configurations by solving numerically Hamilton's equations. Finally, Sec. VI is devoted to summarizing our work and presenting our results.

II. NEMATIC CONFIGURATION

We consider a nematic sphere of radius R which satisfies the weak-anchoring homeotropic boundary conditions [6]. For simplicity we will consider an external field $\mathbf{E}$ which is parallel to the z axis of our system coordinate. Then, if θ is the polar angle with respect to the z axis, one may express the nematic director $\hat{\mathbf{n}}$ in terms of the angle ψ, measured from $\hat{e}_\theta$ and contained in the plane defined by this vector and $\hat{e}_r$, as (see Fig. 1)

$$\hat{\mathbf{n}} = \cos\psi(r,\theta)\hat{e}_r - \sin\psi(r,\theta)\hat{e}_\theta, \tag{1}$$

where r is the radial variable. Notice that by using this ϕ-independent parametrization we are implicitly neglecting

*Corresponding author. FAX: +52 55 56161201. Email address: cmendoza@zinalco.iimatercu.unam.mx

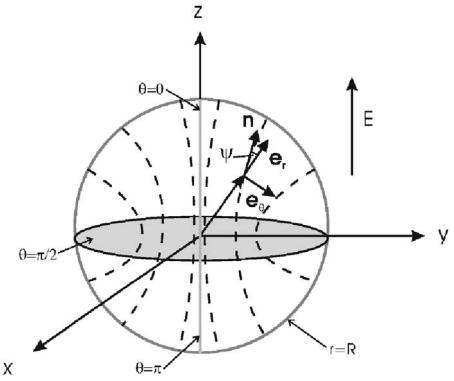

FIG. 1. Schematics of a nematic droplet subject to an external uniform low frequency field. We indicate in gray the regions for which the asymptotic expression for the configuration given by Eq. (6) is exact.

twist deformations. To determine the stable structure of the nematic liquid crystal at constant volume and temperature, we generalize the formalism developed by Kralj *et al.* [7], where they take into account bulk and surface elastic forces as well as external forces. For supramicrometer spheres, far below the nematic-isotropic phase transition, the local biaxial and spatial dependence effects of the nematic order parameter can be neglected [8] and thus the nematic directors, $\hat{\mathbf{n}}$ can be determined by minimizing the Helmholtz free energy $\mathcal{F}$,

$$\mathcal{F} = (RK/2)\int_V ds\, e^{-s} d\Omega \left\{ \left(\frac{\partial\psi}{\partial s}\right)^2 + \left(\frac{\partial\psi}{\partial\theta}\right)^2 + 4\cos^2\psi + \sin^2\psi + \cot^2\theta \sin^2\psi - \sin 2\psi \frac{\partial\psi}{\partial s} - 2(2\cos^2\psi + \sin^2\psi)\frac{\partial\psi}{\partial\theta} + 2\frac{\partial\psi}{\partial s}\cot\theta\sin^2\psi - 2\sin 2\psi\cot\theta + \sin 2\psi\cot\theta\frac{\partial\psi}{\partial\theta} - h^2 e^{-2s}\cos^2(\psi-\theta) - 4\frac{K_{24}}{K}\cos\psi \times\left[\cos\psi + \sin\psi\left(\cot\theta\frac{\partial\psi}{\partial\theta} + \frac{\partial\psi}{\partial s}\right)\right] + \frac{\mu}{R}\sin^2\psi\,\delta(s)\right\}, \quad (2)$$

where Ω is the solid angle, h is a dimensionless field defined by $h^2 \equiv \varepsilon_a E_0^2 R^2/(4\pi K)$ with E_0 the low frequency field amplitude, $s=-\ln(r/R)$, and $\varepsilon_a=\varepsilon_\parallel-\varepsilon_\perp$ the dielectric anisotropy with $\varepsilon_\parallel$ and $\varepsilon_\perp$ the dielectric constants parallel and perpendicular to the optical axis. Here $K=K_1=K_2=K_3$ are the elastic constants in the equal elastic constant approximation, $\mu \equiv RW_0/K_1$, where W_0 is the anchoring strength [9], and we are taking $K_{24}=(K_1+K_2)/2$, as given by the Maier-Saupe molecular approach [10,11]. Finally, we take (splay-bend) $K_{13}\equiv 0$ in agreement to Ref. [11] where the controversy about this constant seems to have been solved. By taking the variational derivative of $\mathcal{F}$, we find for the bulk

$$0 = \frac{\partial^2\psi}{\partial s^2} + \frac{\partial^2\psi}{\partial\theta^2} - \frac{\partial\psi}{\partial s} + \cot\theta\frac{\partial\psi}{\partial\theta} + \sin 2\psi - \frac{\sin 2\psi}{2\sin^2\theta} - 2\cot\theta\sin^2\psi - h^2 e^{2t}\sin 2(\psi-\theta) \quad (3)$$

and for the border $r=R$

$$0 = \frac{\partial\psi}{\partial s} - \cos\psi\sin\psi + \cot\theta\sin^2\psi + \mu\cos\psi\sin\psi + \frac{K_{24}}{K}(\sin 2\psi - \cot\theta\sin^2\psi)\Big|_{r=R}. \quad (4)$$

Equations (3) and (4) have been solved numerically by using a relaxation method [7]. However, since our final aim is to describe the light trajectories within the droplet, it is convenient to have an approximated but analytical solution to establish the governing equation for the ray trajectories.

To find an approximated expression for ψ we use the dominant balance technique [12] which finds the asymptotic behavior of ψ around the singularities of Eq. (3). Notice that this equation shows singularities for $\theta=0$ and $\theta=\pi$ which are located on the sphere diameter parallel to the external field. Since in the vicinity of this diameter $\mathbf{n}$ should be almost aligned with $\mathbf{E}$, ψ is expected to vanish, and since along this diameter $\mathbf{n}$ remains constant, the radial derivatives should satisfy the expressions $(\partial\psi/\partial s)|_{\theta=0,\pi} = (\partial^2\psi/\partial s^2)|_{\theta=0,\pi} = 0$. Under the presence of $\mathbf{E}$, the configuration has azimuthal invariance around the $\mathbf{E}$ direction so that $\psi(\theta)=\psi(-\theta)$ and $\psi(\pi-\theta)=\psi(\pi+\theta)$, which implies that $(\partial^2\psi/\partial\theta^2)|_{\theta=0,\pi}=0$. All these considerations allow us to approximate the last equation around its singularities as

$$\frac{\partial\psi}{\partial\theta} - \frac{\sin 2\psi}{\sin 2\theta} = 0, \quad (5)$$

which can be solved directly, yielding as its general solution

$$\tan\psi = \kappa(s)\tan\theta, \quad (6)$$

where $\kappa(s)$ is an arbitrary function of s which satisfies the boundary conditions

$$[d\kappa(s)/ds + \kappa(s)(\mu+1)/h]_{r=R} = 0 \quad (7)$$

and

$$\kappa(s=\infty) = 1. \quad (8)$$

Here the first condition comes from the radial boundary condition [surface term of Eq. (2)] and the second one guarantees the continuity of ψ at the center. It is important to remark that although this expression was derived around the vicinity of the singularities $\theta=0$ and $\theta=\pi$, it gives the exact value for the equator $\theta=\pi/2$ where $\psi\to\pi/2$, as can be seen by noting that here $(\partial\psi/\partial r)|_{\theta=\pi/2} = (\partial^2\psi/\partial r^2)|_{\theta=\pi/2} = (\partial^2\psi/\partial\theta^2)|_{\theta=\pi/2}=0$ is also satisfied, and thus Eq. (6) does satisfy Eq. (3) as well as in the neighborhood of the equator. The fact that Eq. (6) is a good approximation for the solution of Eq. (3) near $\theta=0$, $\pi/2$, and π makes $\hat{\mathbf{n}}(\theta=0,\pi/2,\pi)$ parallel to $\hat{z}$ on the z axis and on the equator plane for any $\kappa(t)$; which is the expected symmetry for the axial configuration. In summary Eq. (6) is exact at the equator, along the z axis, and at the border of the sphere where the boundary condition is satisfied (see Fig. 1).

III. RADIAL DEPENDENCE

In the preceding section we found the θ dependence of the configuration ψ but the radial dependence remains to be de-

termined. To write an equation for $\kappa(s)$, we insert Eq. (6) into Eq. (2) and minimize the latter equation, following the same steps as in the last section. However, the resulting equation is not autonomous, since it depends explicitly on s, and does not have an analytical solution. In what follows we shall approximate $\kappa(s)$ for intense fields $h \gg 1$.

As is well known, the effect of the external field on the nematic is usually opposed to the elastic force effect, particularly at frontiers of the nematic where the molecules anchor the walls. This effect is stronger for intense $\mathbf{E}$ since in the regions that lie far from the frontier (bulk), the nematic is practically aligned with the field whereas within a layer of nematic in contact with the solid walls, the orientation shows great spatial gradients, such that it reaches the boundary conditions. These two regions with different behaviors can be described simultaneously by using the boundary-layer technique [13,14] for which the bulk is called the exterior region, $\psi_{ext}(z)$, and the region within the layer is called the interior one, $\psi_{in}(z)$. The solutions for both regions are coupled or matched asymptotically to give rise to a uniform solution ψ_{adj} valid for all the domain and is given by

$$\psi_{adj} = \psi_{ext} + \psi_{in} - \psi_{match}, \tag{9}$$

where ψ_{match} is defined by

$$\psi_{match} = \lim_{h\to\infty} \psi_{in} = \lim_{r\to\Upsilon} \psi_{ext}, \tag{10}$$

where Υ represents the region for which ψ_{ext} cannot satisfy at least one of the boundary conditions, which in our case is the border of the droplet, and h is related to the thickness of the interior region or boundary layer.

In order to use this method, we start by approximating the differential equation with respect to a convenient parameter, which in this case is h, which usually reduces the order of the differential equation. Solving this equation, we find the external solution ψ_{ext}, which is not able to satisfy at least one of the boundary conditions. Next, we rewrite the original equation in terms of a scale variable constructed by using h and choosing as spatial scale that which keeps the superior order derivatives even in the limit of large h. The solution of this equation provides us the internal solution $\psi_{in}(h,z)$ which should be able to satisfy that condition which ψ_{ext} cannot satisfy. The final step is to match asymptotically both solutions ψ_{ext} and ψ_{in} to obtain a solution ψ_{adj} valid in the whole domain which according to the boundary-layer theory is given by Eq. (10).

It is illustrative to show that the solution of the corresponding Euler-Lagrange equation associated with Eq. (2) presents boundary-layer behavior [14] for large uniform fields $\mathbf{E}$, by noting that in this case the dominant term of $\mathcal{F}$ is $(\varepsilon_a/4\pi)(\hat{\mathbf{n}}\cdot\mathbf{E})^2 \propto h^2 e^{-2s}\cos^2(\psi-\theta)$ which only minimizes $\mathcal{F}$ when $\hat{\mathbf{n}}$ is parallel to $\mathbf{E}$ ($\psi_{ext} \equiv \theta$). In this way ψ_{ext} describes a uniform configuration (outer solution) and then ψ_{ext} could just satisfy accidentally the radial boundary condition given by the surface terms of Eq. (2). This suggests that in the vicinity of the sphere border the radial variable of the solution (inner solution) should vary with a faster scale.

To study the inner solution ψ_{in}, we introduced the fast variable $t \equiv -h\ln(r/R)$ where h is a dimensionless field. We choose $t \propto h$ because this is the only way in which the maximum power of the rescaled derivative is to be proportional to the same power of h as the external field. Substituting Eq. (6) into Eq. (2) and keeping the dominant terms in h yields

$$\mathcal{F} = (RKh/2)\int_0^\infty dt\, e^{-t/h}\left[e(\kappa_{in}(t))\left(\frac{d\kappa_{in}(t)}{dt}\right)^2 - f(\kappa_{in}(t)) + \delta(t)s(\kappa_{in}(t))\left(\frac{d\kappa_{in}(t)}{dt} + \frac{1+\mu}{h}\kappa_{in}(t)\right) + O\left(\frac{1}{h}\right)\right], \tag{11}$$

where $e(\kappa_{in}(t))$, $f(\kappa_{in}(t))$, and $s(\kappa_{in}(t))$ are given by

$$e(\kappa(t)) \equiv \int_0^\pi \frac{\sin^3\theta\cos^2\theta d\theta}{(\kappa^2\sin^2\theta + \cos^2\theta)^2}, \tag{12}$$

$$f(\kappa(t)) \equiv \int_0^\pi \frac{\sin\theta(\kappa\sin^2\theta + \cos^2\theta)^2}{\kappa^2\sin^2\theta + \cos^2\theta}, \tag{13}$$

and

$$s(\kappa(t)) \equiv \int_0^\pi \frac{\sin\theta[\kappa^2\sin^2\theta + (1-\kappa)\cos^2\theta - \kappa]}{\kappa^2\sin^2\theta + \cos^2\theta}. \tag{14}$$

Although in principle $\kappa_{in}(t)$ is only able to describe the configuration in the boundary layer, the fact that the bulk (outer) configuration $\kappa_{out}(t) \equiv 1$ is a constant and that Eq. (7) is satisfied makes $\kappa_{in}(t)$ indeed the valid solution for κ in the whole domain. The Lagrangian given by Eq. (11) is t independent, and hence has an integration (Euler constant) and is given by $\mathcal{E} = e(\kappa(t))[d\kappa(t)/dt]^2 + f(\kappa(t))$. Notice that when $\kappa(t) = 1$ the nematic is not undistorted; thus the elastic contribution should vanish and $\mathcal{E} = f(1)$. In this way the solution of this equation that satisfies the boundary condition $d\kappa(0)/dt + \kappa(0)(\mu+1)/h = 0$ is given by

$$\frac{1}{h}\ln\left(\frac{r}{R}A\right) = \int^{k_3} \frac{dk}{\sqrt{\kappa}(1-\kappa)} \sqrt{\frac{-3\kappa + \frac{2\kappa^2+1}{\sqrt{1-\kappa^2}}\arctan\left(\frac{\sqrt{1-\kappa^2}}{\kappa}\right)}{\frac{4+2\kappa^2}{3} - 2\kappa\frac{\arctan(\sqrt{1-\kappa^2}/\kappa)}{\sqrt{1-\kappa^2}}}}. \tag{15}$$

Here $\kappa(0) \equiv k_0[(\mu+1)/h]$ is only a function of $(\mu+1)/h$ because the boundary condition can be written as an algebraic function of $\kappa(0)$. In Eq. (15) we have separated explicitly the poles of the integrand whereas the remaining expression behaves like a constant. Thus, it is a good approximation to replace it by 1 so that Eq. (15) turns out to be

$$\frac{1}{h}\ln\left(\frac{r}{R}A\right)=\int^{\kappa_3}\frac{d\kappa}{\sqrt{\kappa}(1-\kappa)}=\ln\left(\frac{1-\sqrt{\kappa_2}}{1+\sqrt{\kappa_2}}\right). \quad (16)$$

This can be checked quantitatively by performing the numerical integral $\int_0^1[r(\kappa_2)-r(\kappa_3)]^2dk/A\approx 7.2\times 10^{-5}$, which shows that these functions are really close in the whole interval. Solving Eq. (16) for k_2 we obtain

$$\kappa_2(r)=\left(\frac{1-B(r/R)^h}{1+B(r/R)^h}\right)^2, \quad (17)$$

where $B=(1-\sqrt{\kappa_0})/(1+\sqrt{\kappa_0})$ and

$$k_0=-\sqrt{(1+(1+\mu)^2/2h^2)^2-1}+1+(1+\mu)^2/2h^2$$

.

To illustrate graphically the behavior of this configuration, we substitute κ in Eq. (6) which in turn we substitute in Eq. (1), to obtain the following result:

$$\hat{\mathbf{n}}=\frac{2(\rho^2+z^2)^h z\rho\hat{e}_\rho+\{[1+(\rho^2+z^2)^h]z^2+\rho^2[1-(\rho^2+z^2)^h]\}\hat{k}}{\sqrt{\rho^2+z^2}\sqrt{z^2[1+(\rho^2+z^2)^h]^2+\rho^2[1-(\rho^2+z^2)^h]^2}} \quad (18)$$

where $z=(r/R)\cos\theta$ and $\rho=(r/R)\sin\theta$ are the cylindrical coordinates and $\hat{e}_\rho$ and $\hat{k}$ are the unit vectors in the ρ direction and in the z direction, respectively. We can exhibit geometrically the nematic configuration if we define the director lines as follows:

$$\frac{d\rho}{dz}=\frac{n_\rho}{n_z}=2z\rho/\{[1+(\rho^2+z^2)^{-h}]z^2+\rho^2[(\rho^2+z^2)^{-h}-1]\}. \quad (19)$$

Similarly as the electrostatic field lines are defined, $\hat{\mathbf{n}}$ is parallel to the tangent to the curve which touches the point where $\hat{\mathbf{n}}$ is to be calculated. The insets of Figs. 3 below show some curves obtained from Eq. (19) which are depicted for equidistant angles on the droplet frontier for various values of h in increasing order. It can be seen, as should be expected, that the curves are more aligned with the field for larger values of h. It is known that for strong enough external fields and strong enough anchoring, there exists a singular ring located at the equator of the droplet ($\rho=1, z=0$). This can be shown from our expression for the director, Eq. (18), which was derived assuming a strong electric field. Indeed, if we set $\rho=1$ and $z=0$ in this equation, we get an undefined director which confirms the existence of the singular ring.

IV. TRANSVERSE MAGNETIC AND ELECTRIC EIKONALS

Electromagnetic field propagation for anisotropic inhomogeneous media has been extensively studied. In fact, for the case of stratified media, it has been utilized different procedures for solving this problem. One of the most widely used procedures is the so called Berreman formalism [15], which is very useful for solving problems where the configuration is one-variable dependent. There are also some other more restricted methods than the asymptotic ones, like the quasi-isotropic approximation. A review paper of these formalisms is given by [16]. There are, as well, general formalisms for describing both the propagation of acoustic [17] and electromagnetic [18] waves in this kind of medium, which are based on eikonal dyads. However, these formalisms do not take advantage of the complete representation in terms of the transverse magnetic (TM) modes and the transverse electric (TE) modes which simplifies greatly the description of nonmagnetic media [20]. From Maxwells equations the TE eikonal equation was derived and is given by

$$[\nabla\mathcal{L}_{\mathrm{TE}}(\mathbf{r})\times\hat{\mathbf{e}}]^2=\mu\varepsilon_{ee}, \quad (20)$$

where $\hat{\mathbf{e}}=\mathbf{e}(\mathbf{r})/e$, with $\mathbf{e}(\mathbf{r})$ the electric field amplitude whose magnitude is e and $\varepsilon_{ee}=\hat{\mathbf{e}}\cdot\overleftrightarrow{\varepsilon}\cdot\hat{\mathbf{e}}$, μ the magnetic permeability, and $\mathcal{L}$ the optical path between two fixed points. As can be seen from Eq. (20), it only involves consistently components of $\nabla\mathcal{L}(\mathbf{r})$ perpendicular to $\hat{\mathbf{e}}$. Complementarily, the corresponding magnetic field for these modes, which is also transverse, should be obtained from

$$\mathbf{h}(\mathbf{r})=\nabla\mathcal{L}_{\mathrm{TE}}(\mathbf{r})\times\mathbf{e}(r)/\mu. \quad (21)$$

The eikonal equation for the TM modes is given by [20]

$$(\nabla\mathcal{L}_{\mathrm{TM}}\times\hat{\mathbf{h}})\cdot\overleftrightarrow{\varepsilon}^{-1}\cdot(\nabla\mathcal{L}_{\mathrm{TM}}\times\hat{\mathbf{h}})=\mu, \quad (22)$$

where $\hat{\mathbf{h}}=\mathbf{h}/|\mathbf{h}|$. Similarly, this equation only involves components of $\nabla\mathcal{L}(\mathbf{r})$ perpendicular to $\hat{\mathbf{h}}$ but in contrast to the TE modes, the corresponding electric fields are not transverse, as is evident from

$$\mathbf{e}=-\overleftrightarrow{\varepsilon}^{-1}\cdot\nabla\mathcal{L}_{\mathrm{TM}}\times\mathbf{h}. \quad (23)$$

It is worthwhile to rewrite the eikonal equations (20) and (22) in terms of the orthogonal coordinate system $\{q_1,q_2,q_3\}$. For a given q_1 along $\hat{\mathbf{h}}$ and $\hat{\mathbf{e}}$ we have that Eqs. (20) and (22) turn out to be

$$\frac{1}{h_2^2}\left(\frac{\partial\mathcal{L}_{\mathrm{TE}}}{\partial q_2}\right)^2+\frac{1}{h_2^3}\left(\frac{\partial\mathcal{L}_{\mathrm{TE}}}{\partial q_3}\right)^2=\mu\varepsilon_{11}, \quad (24)$$

and

$$\frac{\varepsilon_{22}^{-1}}{h_3^2}\left(\frac{\partial\mathcal{L}_{\mathrm{TM}}}{\partial q_3}\right)^2-\frac{2\varepsilon_{23}^{-1}}{h_2h_3}\left(\frac{\partial\mathcal{L}_{\mathrm{TM}}}{\partial q_2}\right)\left(\frac{\partial\mathcal{L}_{\mathrm{TM}}}{\partial q_3}\right)+\frac{\varepsilon_{33}^{-1}}{h_2^2}\left(\frac{\partial\mathcal{L}_{\mathrm{TM}}}{\partial q_2}\right)^2=\mu. \quad (25)$$

Here h_i ($i=2,3$) are scale factors and ε_{ij}^{-1} are the elements of $\overleftrightarrow{\varepsilon}^{-1}$. We should remark that the ordinary or TE rays propagate as in an isotropic medium with effective refraction index $n^2=\mu\varepsilon_{11}$ whereas the extraordinary or TM rays are governed by a bilinear nondiagonal form for the ray components $p_i=\partial\mathcal{L}/\partial q_i$. Similar results have been found in the context of geometrical acoustics where there exist three different polarizations: one quasilongitudinal and two quasitransverse which in the general case cannot be decoupled [19].

V. RAY TRACING

The TM eikonal for the radial configuration can be solved analytically [21]. However, for the configuration in the pres-

ence of field the situation is different since ψ depends on two independent variables r and θ and it is therefore convenient to use an alternative Hamiltonian representation. Under this formalism we replace a partial differential equation of first order by a system of ordinary differential equations. The equivalence between both representations not only is well established in optics, but is valid in general in the context of partial differential equations [22].

The relevant components of the dielectric tensor are given by $\varepsilon_{rr}=\varepsilon_\perp+\varepsilon_a\cos^2\psi(x,\theta)$, $\varepsilon_{r\theta}=-\varepsilon_a\sin\psi(x,\theta)\cos\psi(x,\theta)$, and $\varepsilon_{\theta\theta}=\varepsilon_\perp+\varepsilon_a\sin^2\psi(x,\theta)$ which are functions of θ and $x=r/R$. Also, we identify $p=\partial\mathcal{L}_{\mathrm{TM}}/\partial r$ and $q=\partial\mathcal{L}_{\mathrm{TM}}/\partial\theta$ as the ray radial and angular components and $H=\varepsilon_\perp\varepsilon_\parallel$ as the Hamiltonian of the system. In terms of these variables Eq. (25) takes the form

$$\varepsilon_{rr}p^2+2\frac{\varepsilon_{r\theta}}{x}pq+\frac{\varepsilon_{\theta\theta}}{x^2}q^2=H, \tag{26}$$

from which we can obtain the ray trajectories within the droplet by using the Hamilton equations [23] given by

$$\frac{\partial H}{\partial p}=\frac{dx}{d\tau},\quad \frac{\partial H}{\partial x}=-\frac{dp}{d\tau}, \tag{27}$$

$$\frac{\partial H}{\partial\theta}=-\frac{dp}{d\tau},\quad \frac{\partial H}{\partial q}=\frac{d\theta}{d\tau}, \tag{28}$$

where τ is the parameter of the curve. Inserting Eq. (26) into the three first of the Hamilton equations, we arrive at

$$\frac{dx}{d\tau}=2p\varepsilon_{rr}+\frac{2\varepsilon_{r\theta}}{x}q, \tag{29}$$

$$x\frac{d\theta}{d\tau}=2p\varepsilon_{r\theta}+2\varepsilon_{\theta\theta}\frac{q}{x}, \tag{30}$$

$$\frac{dq}{d\tau}=\varepsilon_a\frac{[(p^2-q^2/x^2)\sin 2\psi+(2qp\cos 2\psi)]}{\cos^2\theta+\kappa(x)^2\sin^2\theta}\kappa(x), \tag{31}$$

where we have used Eq. (6) to simplify the last equation. Here, we have not used the last Eq. (28) since one of the four variables p,q,r, and θ is dependent on the others through Eq. (26). For instance we can write p as

$$p=-\frac{\varepsilon_{r\theta}}{x\varepsilon_{rr}}q\pm\frac{\sqrt{\varepsilon_\perp\varepsilon_\parallel(\varepsilon_{rr}x^2-q^2)}}{x\varepsilon_{rr}}. \tag{32}$$

Notice that this expression provides real values of p when $\varepsilon_{rr}x^2-q^2\geqslant 0$ where the equality defines the locus of the turning points of the trajectories or caustics. Thus, after substituting ε_{rr} and Eq. (6) it leads to

$$\tan\theta=\frac{1}{\kappa(x)}\sqrt{\frac{\varepsilon_\parallel x^2-q^2}{q^2-\varepsilon_\perp x^2}}. \tag{33}$$

It is important to stress that each sign of Eq. (32) corresponds to one of the two branches of the trajectory that result when this reaches the turning point or touches tangentially the caustic. Thus, for a specific parametrization, one sign describes the incident ray and the other the emerging one. To find the ray trajectories, we solve numerically the system defined by Eqs. (29)–(31) for θ, r, and q by using the Runge-Kutta method. The initial conditions are the position in polar coordinates (R,θ_0) that we chose in the border of the droplet and q at the same point, which is related to the incident angle by

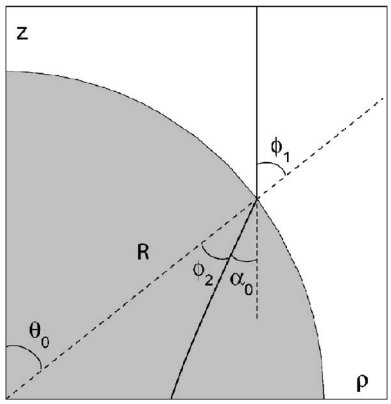

FIG. 2. The angular coordinate of the point of incidence θ_0 and the angle α_0 between the trajectory just entering the droplet and the z axis. We also show the angle of incidence ϕ_1 and the refracted angle ϕ_2.

$$q_0=\frac{\sqrt{\varepsilon_\perp}|\sin(\alpha_0-\theta_0)|}{\sqrt{(\varepsilon_\perp/\varepsilon_\parallel)\cos^2(\alpha_0-\theta_0)+\sin^2(\alpha_0-\theta_0)}}. \tag{34}$$

In this equation α_0 is the angle between the z axis and the trajectory just inside the droplet (see Fig. 2). Since we are assuming that the plane wave is coming from an isotropic medium, we have to take into account the ray deviation at the frontier between both media. After imposing the corresponding boundary conditions for a superposition of plane wave electromagnetic fields, it can be shown that the component of the wave vector parallel to the interface is conserved [24], which mathematically can be expressed as

$$\mathbf{k}_1\cdot\mathbf{r}|_{\mathrm{sup}}=\mathbf{k}_2\cdot\mathbf{r}|_{\mathrm{sup}}, \tag{35}$$

where $\mathbf{k}_1$ and $\mathbf{k}_2$ are the wave vectors in the media 1 and 2. Because this equation is satisfied on the surface, $\mathbf{r}$ should lie there and the components of $\mathbf{k}_1$ and $\mathbf{k}_2$ parallel to the frontier are conserved. For the nematic droplet k_θ and k_r are the ray components parallel and perpendicular to the homeotropically aligned droplet surface; thus the eikonal equation Eq. (25) on the surface takes the form

$$\varepsilon_\parallel k_r^2+\frac{\varepsilon_\perp k_\theta^2}{x^2}=\varepsilon_\parallel\varepsilon_\perp, \tag{36}$$

where the components of the wave vector can be written in terms of the angle formed by the ray within the droplet and the inward normal to the surface ϕ_2 as

$$k_r=|k|\cos\phi_2,\quad k_\theta=|k|\sin\phi_2. \tag{37}$$

By substituting these components into Eq. (36), we have

$$k_\theta=\frac{\sqrt{\varepsilon_\parallel\varepsilon_\perp}\sin\phi_2}{\sqrt{\varepsilon_\parallel\cos^2\phi_2+\varepsilon_\perp\sin^2\phi_2}}. \tag{38}$$

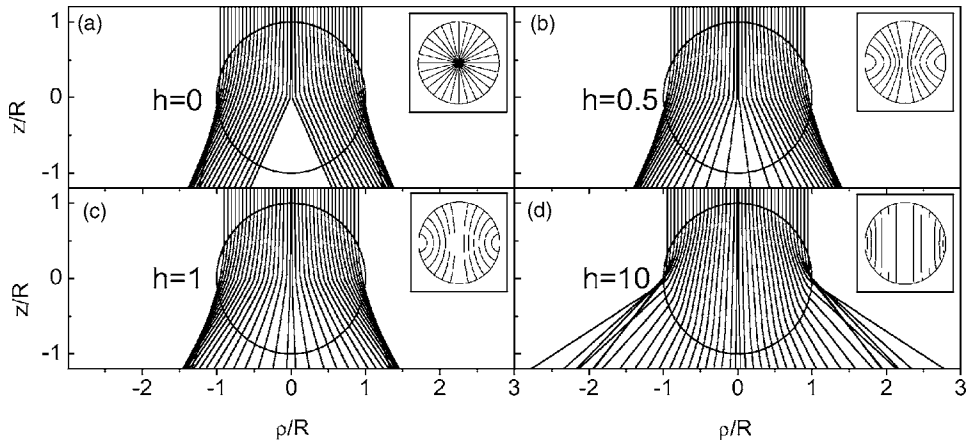

FIG. 3. Ray trajectories of a set of initially parallel rays entering a droplet for various values of h. The insets show the director lines acquired by the nematic for the same values of h. The dielectric constants are $\varepsilon_{\parallel}=1.8$ and $\varepsilon_{\perp}=1.3$ which corresponds to 5 CB at a wavelength of 632 nm and at a temperature of 25 °C.

Inserting this value of k_θ into Eq. (35) we obtain the equation that plays the role of Snell's law for isotropic media,

$$\sqrt{\varepsilon_h}\sin\phi_1 = \frac{\sqrt{\varepsilon_{\parallel}\varepsilon_{\perp}}\sin\phi_2}{\sqrt{\varepsilon_{\parallel}\cos^2\phi_2 + \varepsilon_{\perp}\sin^2\phi_2}}, \tag{39}$$

where ϕ_1 is the angle formed between the ray in the matrix and the outward normal to the surface (see Fig. 2) and $\sqrt{\varepsilon_h}$ is the refraction index in the same medium that we have indicated by 1. It is important to remark that we have restricted our derivation to the case of a droplet having a homeotropic alignment, that is to say, this expression only describes the case when the optical axis of the nematic has homeotropic boundary conditions. The boundary condition for the general case also can be deduced from Eq. (26) but we do not need it for the present study.

Using Eq. (39) we can calculate the angle α_0 in Eq. (34) considering that the incident ray is parallel to the z axis. It leads to

$$\alpha_0 = \pi/2 - \theta_0 - \arcsin\left(\frac{\sqrt{\varepsilon_{\perp}}\cos\theta_0}{\sqrt{\varepsilon_{\parallel}\varepsilon_{\perp}/\varepsilon_h + \varepsilon_a\cos^2\theta_0}}\right).$$

Figure 3 shows the trajectories when the rays of a plane wave front, coming from an isotropic medium of dielectric constant $\varepsilon_h=\varepsilon_{\parallel}$ whose wave vector is parallel to the low frequency electric field, cross a nematic droplet and emerge from it with an emerging angle γ. For different values of h, it can be observed how the shadow cone which stands under the droplet when no field is applied vanishes when a field is imposed. Moreover, the ray deviations diminish for larger values of h. We should mention that the rays crossing the droplet almost by the border are the most deviated because of the hard anchoring condition we used to calculate the configuration. Hence, we expect that those rays will be less deviated when replacing the latter condition by a more realistic weak anchoring condition. In Fig. 4 is plotted the ray deviation as a function of the impact parameter x_{in} parametrized by the external field. We note that for $h=0$ this deviation exhibits a minimum even for the rays crossing through the center of the droplet, whereas this minimum value vanishes for any value of h different from zero.

It is also interesting to remark that near the center of the droplet, the derivative of γ decreases as we incease the values of h. However, near the border of the droplet, this derivative increases with increasing h. This is clearly shown for $h=10$ and is mainly due to the hard anchoring boundary condition we are using.

VI. CONCLUDING REMARKS

Here, we found an asympotic analytical expression for describing the axial configuration obtained after applying to the droplet a low frequency electric field with hard anchoring homeotropic boundary conditions. This expression is exact in certain regions of the droplet: the equator plane, the field axis, and the border of the sphere. We also calculated the radial dependence of the configuration by using the boundary-layer technique.

The analytical configuration we found satisfies topological conservation laws [25] because for a nonvanishing field, it exhibits a ring disclination at the equator while for a vanishing field it reduces to the radial configuration showing a point defect at the center.

Next, we found the ray trajectories of rays corresponding to an initially plane wave coming from an isotropic medium

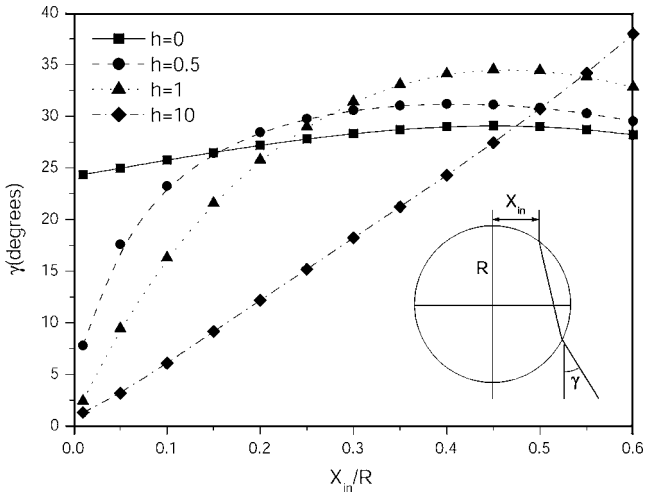

FIG. 4. Deviation angle γ as a function of the incidence impact parameter x_{in} parametrized by h.

surrounding the droplet, crossing the droplet, and returning to the isotropic medium. We made this for various nematic configurations associated with different magnitudes of low frequency fields. These results allowed us to show that a nematic droplet in the absence of a low frequency field deflects the rays crossing the droplet, leaving a shadow below it. On the other hand, when the droplet is under the action of a low frequency field, the shadow disappears and the rays suffer a smaller deflection which diminishes for larger low frequency fields.

Thus, if a wave front is to traverse a structure having a random arrangement of nematic droplets, the deflection of the rays in the absence of the low frequency field will repeat every time the light crosses each droplet, so that after many droplets the wave front will be divided into pieces, each one propagating in a different direction. Hence, the wave front with defined phase and direction will be scattered and no image will be seen through the matrix with droplets. In contrast, when the field is applied, a large portion of the rays will not be deviated from their initial direction so that they retain their phase and direction after crossing the matrix with droplets, which therefore appears as a transparent medium. Thus, these results are consistent with observed phenomenology of the electro-optical effect in PDLC cells which scatter light in the absence of applied fields while they become transparent under the action of the field.

In contrast to other approaches, our analysis takes into account explicitly the refractive effects within the droplet by using the eikonal formulation valid in the optical limit. Since in our results we obtain detailed information of the trajectory, we can calculate the precise optical paths of the incident wave front and therefore the diffraction spectra and transmittance as a function of the applied field. This could be useful for the design of optical devices.

[1] J. W. Doane, N. A. Vaz, B.-G. Wu, and S. Zumer, Appl. Phys. Lett. **48**, 269 (1986); J. W. Doane, MRS Bull. **16**, 22 (1991).
[2] M. Schadt, Liq. Cryst. **14**, 73 (1993).
[3] H. S. Kitzerov, Liq. Cryst. **16**, 1 (1994).
[4] S. Zumer and J. W. Doane, Phys. Rev. A **34**, 3373 (1986).
[5] S. Zumer, Phys. Rev. A **37**, 4006 (1988).
[6] E. Santamato, G. Abbate, P. Maddalena, L. Marrucci, and Y. R. Shen, Phys. Rev. Lett. **64**, 1377 (1990); G. Abbate, P. Maddalena, L. Marrucci, L. Saetta, and E. Santamato, J. Phys. II **1**, 543 (1991).
[7] S. Kralj and S. Zumer, Phys. Rev. A **45**, 2461 (1992).
[8] D. W. Allender, G. L. Henderson, and D. L. Johnson, Phys. Rev. A **24**, 1086 (1981).
[9] H. Yokoyama, S. Kobayashi, and H. Kamei, J. Appl. Phys. **61**, 4501 (1987).
[10] J. Nehring and A. Saupe, J. Chem. Phys. **54**, 337 (1971); **56**, 5527 (1972).
[11] H. Yokoyama, Phys. Rev. E **55**, 2938 (1997).
[12] D. Zwillinger, *Handbook of Differential Equations* (Academic Press, New York, 1989).
[13] H. Schlichting, *Boundary Layer Theory* (McGraw-Hill, New York, 1968).
[14] M. C. Bender and M. C. Arszog, *Advanced Mathematical Methods for Scientists and Engineers* (McGraw-Hill, New York, 1978), Sec. 9.2.
[15] D. W. Berreman, J. Opt. Soc. Am. **62**, 502 (1972).
[16] Y. A. Kratsov, O. N. Naida, and A. A. Fuki, Phys. Usp. **39**, 129 (1996).
[17] L. M. Barkovskii and Tkhi Nguet Khan, Sov. Phys. Acoust. **36**, 550 (1990).
[18] L. M. Barkovskii and Tkhi Nguet Khan Fo, Opt. Spectrosc. **70**, 34 (1991).
[19] I. V. Fedorov, *Theory of Elastic Waves in Crystals* (Nauka Press, Moscow, 1965).
[20] J. A. Reyes, J. Phys. A **32**, 3409 (1999).
[21] J. A. Reyes, Phys. Rev. E **57**, 6700 (1998).
[22] I. N. Sneddon, *Partial Differential Equations* (McGraw-Hill, New York, 1957), Sec. 2.10.
[23] H. Goldstein, *Classical Mechanics* (Addison-Wesley, Reading, MA, 1975).
[24] E. Hecht and A. Zajac, *Optics*, 2nd ed. (Addison-Wesley, Reading, MA, 1974), Sec. 4.3, p. 92.
[25] M. Kleman and O. D. Lavrentovich, *Soft Matter Physics* (Springer, New York, 2003).